

promoting access to White Rose research papers



Universities of Leeds, Sheffield and York
<http://eprints.whiterose.ac.uk/>

This is the version of an article published in **Physical Review Letters**

White Rose Research Online URL for this paper:

<http://eprints.whiterose.ac.uk/id/eprint/75645>

Published article:

Wang, LW, Califano, M, Zunger, A and Franceschetti, A (2003) *Pseudopotential theory of Auger processes in CdSe quantum dots*. Physical Review Letters, 91 (5). 564041 - 564044 . ISSN 0031-9007

<http://dx.doi.org/10.1103/PhysRevLett.91.056404>

Pseudopotential Theory of Auger Processes in CdSe Quantum Dots

Lin-Wang Wang

Computational Research Division, Lawrence Berkeley National Laboratory, Berkeley, California 94720, USA

Marco Califano and Alex Zunger

National Renewable Energy Laboratory, Golden, Colorado 80401, USA

Alberto Franceschetti

Oak Ridge National Laboratory, Oak Ridge, Tennessee 37831, USA

(Received 15 October 2002; published 31 July 2003)

Auger rates are calculated for CdSe colloidal quantum dots using atomistic empirical pseudopotential wave functions. We predict the dependence of Auger electron cooling on size, on correlation effects (included via configuration interaction), and on the presence of a spectator exciton. Auger multiexciton recombination rates are predicted for biexcitons as well as for triexcitons. The results agree quantitatively with recent measurements and offer new predictions.

DOI: 10.1103/PhysRevLett.91.056404

PACS numbers: 71.15.-m, 71.55.-i

Auger effects are expected to play a central role in carrier relaxation in nanostructures [1–9]. Two types of Auger effects, illustrated in Fig. 1, are prominent.

(i) *Electron cooling* [Figs. 1(a) and 1(b)]: In the 3D bulk, or a 2D quantum well, the relaxation of an excited electron to its ground state usually occurs by phonon emission. The discrete nature of the electronic states of 0D dots is expected [2] to prevent phonon-assisted electron relaxation (phonon bottleneck). Multiphonon (combined LO \pm LA) [3] or polaronic [4,5] effects may allow electronic relaxation to occur within a limited energy range around the phonon energy $\hbar\omega_0$. However, this may not be sufficient to remove the phonon bottleneck in small, strongly confined quantum dots (QDs). On the other hand, electron relaxation rates in CdSe QDs were observed to be fast ($\tau \sim 0.3$ ps in 2.3 nm radius nanocrystals [6], $\tau = 0.9$ –1.2 ps for samples of size 4.3 nm [7]). It was proposed [8] that in a photoexcited QD the “hot” electron can transfer its energy to the hole via an Auger process involving electron-hole scattering.

(ii) *Auger multiexciton recombination* [Figs. 1(c) and 1(d)]: A ground-state biexciton can decay into an excited-state monoexciton. Because of a large number of final excited states, the efficiency of this process competes with radiative recombination and effectively quenches the photoluminescence intensity [9]. The inverse Auger process (creation of two e - h pairs from a single excited exciton) has been advocated [10] as a mechanism of enhancing solar cell efficiency. A similar Auger process involves the decay of a ground-state triexciton into an excited biexciton; this $3 \rightarrow 2$ Auger decay [Fig. 1(d)] can be even faster than the $2 \rightarrow 1$ decay [Fig. 1(c)]. Yet another type of Auger process involves the decay of a ground-state trion into a hot electron [Fig. 1(e)] or a hot hole [Fig. 1(f)].

All Auger effects illustrated in Fig. 1 are at the heart of QD carrier dynamics, and produce phenomena distinct from bulk physics. Recently, femtosecond carrier dynam-

ics studies (see [1,6,9] and references therein) have been performed on colloidal QDs. These experiments have revealed various carrier relaxation phenomena, which have been attributed to different Auger processes.

We have applied our empirical pseudopotential many-body approach [11] to calculate different Auger processes in CdSe QDs. We show that such calculations produce quantitative agreement with experiments, reveal the dependence of cooling rates on exciton energy and on the

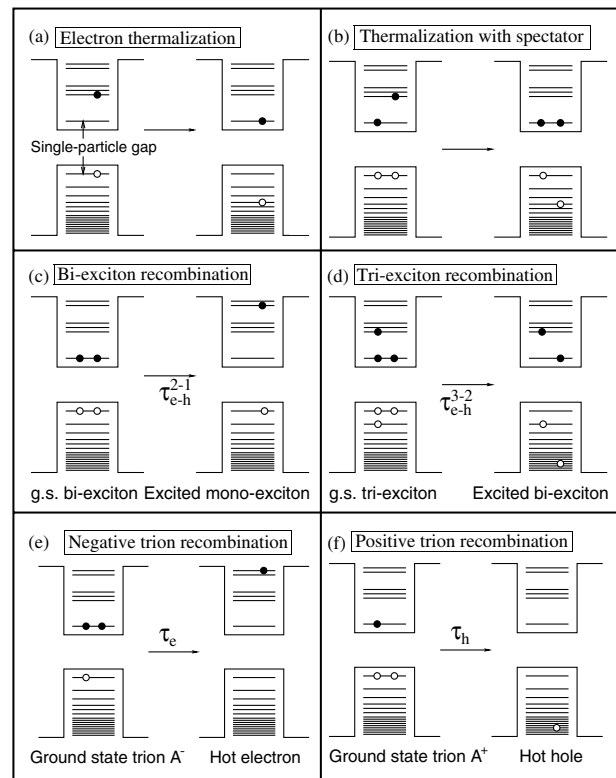


FIG. 1. Illustration of the Auger processes considered here.

presence of additional (“spectator”) charges, and predict the ratios between $\tau_{e-h}^{3\rightarrow 2}$ and $\tau_{e-h}^{2\rightarrow 1}$, the relations between $\tau_{e-h}^{2\rightarrow 1}$ and τ_e and τ_h , and the role of the dot surface in Auger multiexciton recombination.

Method of calculation.—Although there is no wave vector momentum conservation in Auger processes for a QD, the energy still needs to be conserved. The discreteness of the dot-confined single-particle energy levels would seem to preclude energy conservation and therefore efficient Auger transitions [12]. However, other interactions having quasicontinuous spectra (e.g., phonons) can be involved and thus mitigate the energy conservation problem. We consider Auger final states with a finite lifetime \hbar/Γ [thus evolving with time as $\Phi_f \exp(-i\omega t - \Gamma t/2\hbar)$] to account for these interactions, which may cause their decay into lower energy states. We derive a phenomenological formula for the Auger rate (under the standard time-dependent perturbation theory):

$$W_i = \frac{\Gamma}{\hbar} \sum_n \frac{| \langle i | \Delta H | f_n \rangle |^2}{(E_{f_n} - E_i)^2 + (\Gamma/2)^2}, \quad (1)$$

where $|i\rangle$ and $|f_n\rangle$ are the initial and final Auger electronic states, E_{f_n} and E_i are their eigenenergies, and ΔH is the Coulomb interaction. In Eq. (1), we have used multiple final states $\{n\}$ (where n includes spin as well), since each final state might have some contributions to the Auger rate $W = 1/\tau$. For $T \neq 0$ we take a Boltzmann average over the initial states. The single-particle energy levels ϵ_i were computed with the plane-wave empirical pseudopotential method (EPM) described in Ref. [13] and solved within a plane-wave basis, including spin-orbit effects. The surface of the wurtzite spherical dots is saturated by ligand potentials [14]. We have used the EPM of Ref. [15], both with the original G -space numerical implementation of the nonlocal potential [15] (EPM-1) and with a real-space implementation [16] (EPM-2), necessitated by the adaptation to a massively parallel computational platform. The Auger matrix elements obtained with EPM-1 and EPM-2 differ by less than 5%. We consider two dots, $\text{Cd}_{232}\text{Se}_{235}$ and $\text{Cd}_{534}\text{Se}_{527}$, of diameters 29.25 and 38.46 Å, respectively. The initial and final states $|i\rangle$ and $|f\rangle$ are given by Slater determinants obtained by populating the appropriate electronic states. When the initial or final states are degenerate or nearly degenerate, a configuration-interaction (CI) expansion of the many-body states was used to account for the coupling between the nearly degenerate Slater determinants. The evaluation of the Auger matrix elements $\langle i | \Delta H | f \rangle$ requires the calculation of Coulomb integrals of the form

$$J(j, k, l, m) = \sum_{\sigma, \sigma'} \iint \phi_j^*(\mathbf{r}, \sigma) \phi_k^*(\mathbf{r}', \sigma') \frac{e^2}{\bar{\epsilon}(\mathbf{r}, \mathbf{r}') |\mathbf{r} - \mathbf{r}'|} \times \phi_l(\mathbf{r}, \sigma) \phi_m(\mathbf{r}', \sigma') d^3 r d^3 r', \quad (2)$$

where $\{\phi_i\}$ are the single-particle wave functions and $\bar{\epsilon}(\mathbf{r}, \mathbf{r}')$ is the dielectric function of the QD.

Traditionally, in the theoretical treatment of *bulk* Auger processes, the Coulomb integrals are fully screened [17]. In a QD it is important to determine whether the main contribution to a particular set of $J(j, k, l, m)$ (and therefore to a particular Auger process) comes from the interior of the dot [in which case screening $\bar{\epsilon}(\mathbf{r}, \mathbf{r}') \neq 1$ might be important], or from its surface [in which case $\bar{\epsilon}(\mathbf{r}, \mathbf{r}') \sim 1$ would be a reasonable approximation]. To account for both possibilities, we use a dielectric screening function:

$$\frac{1}{\bar{\epsilon}(\mathbf{r}, \mathbf{r}')} = 1 + \left(\frac{1}{\bar{\epsilon}_{in}(\mathbf{r}, \mathbf{r}')} - 1 \right) m(r) m(r'), \quad (3)$$

where $m(r)$ is a mask function that changes smoothly from 1, when r is inside the dot, to 0, when r is outside. $\bar{\epsilon}(\mathbf{r}, \mathbf{r}')$, therefore, is equal to $\bar{\epsilon}_{in}(\mathbf{r}, \mathbf{r}')$ inside the dot, while it is equal to 1 when r or r' or both are outside. Equation (3) can thus also be used to investigate the origin (surface or interior) of the integrals $J(j, k, l, m)$: if its use yields a result that is close to that obtained with $\bar{\epsilon}(\mathbf{r}, \mathbf{r}') = \bar{\epsilon}_{in}(\mathbf{r}, \mathbf{r}')$ [$\bar{\epsilon}(\mathbf{r}, \mathbf{r}') = 1$], then the main contribution to the integrals comes from the interior [surface] of the dot.

Auger electron thermalization.—The final and critical step in the electron cooling process [Fig. 1(a)] involves the decay of the excited electron from the p level e_p to the ground electronic state e_s . In the Auger-mediated thermalization process, this is achieved by promoting a hole from h_s to h_n . The decay rate is thus

$$\tau^{-1} = \frac{\Gamma}{\hbar} \sum_{n\alpha} \frac{|J(h_s, e_p; h_n, e_{s,\alpha})|^2}{(\Delta E + \epsilon_{h_n} - \epsilon_{h_s})^2 + (\Gamma/2)^2}, \quad (4)$$

where $\Delta E = \epsilon_{e_p} - \epsilon_{e_s}$ is the energy difference between initial and final electron levels and the sum runs over the spin $\alpha = \uparrow, \downarrow$ of the s electron as well. Using the masked dielectric function of Eq. (3), we find that the main contribution to the integrals $J(h_s, e_p, h_n, e_s)$ comes from the interior of the dot. Therefore the use of $\bar{\epsilon}(\mathbf{r}, \mathbf{r}') = \bar{\epsilon}(d; |\mathbf{r} - \mathbf{r}'|)$ [where $\bar{\epsilon}(d; |\mathbf{r} - \mathbf{r}'|)$ is our calculated dielectric function [15] which depends on the dot size d] is appropriate for the Auger thermalization process. The summation in Eq. (4) includes 30 final hole states $\{\phi_{h_n}\}$ [18]. Since in actual nanocrystals, there are many factors which might affect the value ΔE of the electron sp splitting (shape and size distribution, surface effects, external charge near the QD, etc.), in Fig. 2 $\tau^{-1}(h_s, e_p \rightarrow h_n, e_s)$, calculated for $T = 0$ K, is plotted as a function of ΔE , for three possible values (5, 10, and 20 meV) of the broadening Γ [19]. We find that at resonance [i.e., when $\Delta E \sim \epsilon_{h_s} - \epsilon_{h_n}$ and $J(h_s, e_p, h_n, e_s)$ is large], τ is of the order of 0.1 ps, whereas away from resonance, the Auger lifetime is inversely proportional to Γ , and, for $\Gamma = 10$ meV, τ is about 0.5 ps for both QDs. These results are in excellent agreement with a recent experiment by Klimov [1], where the p to s electron cooling has been determined to have a lifetime of 0.12 and 0.25 ps for nanocrystals with $R = 17$ and 23 Å, respectively. Auger

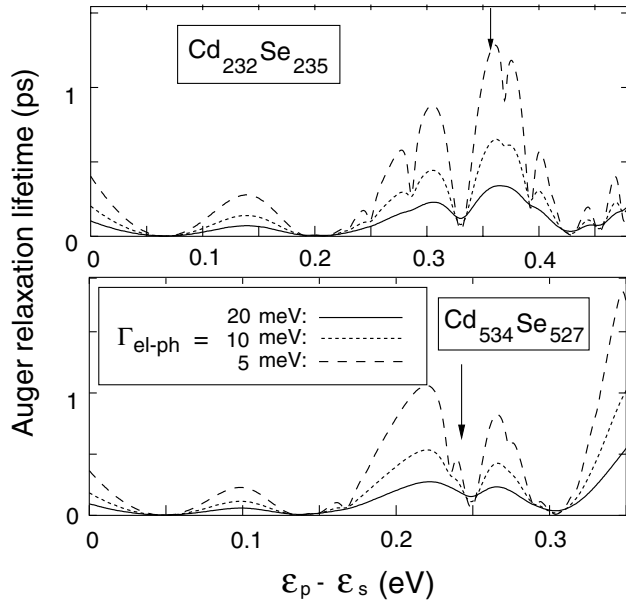


FIG. 2. Auger lifetimes for *electron cooling*, evaluated at $T = 0$ K, with EPM-2 and within the single-particle approximation, for three values of the broadening parameter Γ [see Eq. (4)]. The vertical arrows denote the value of the calculated cooling energy $\Delta E = \epsilon_{e_p}^0 - \epsilon_{e_s}^0$.

effects in QDs have been previously modeled using $\mathbf{k} \cdot \mathbf{p}$ [8,12] and tight-binding [21] Hamiltonians. The most recent calculation of Auger rates in CdSe nanocrystals [8] predicted, using $\mathbf{k} \cdot \mathbf{p}$, an Auger lifetime for the relaxation from the $1P$ to the $1S$ electron level of $\tau = (2.1 \pm 0.2)$ ps, almost constant over the range of radii from 20 to 40 Å. This value overestimates our results by a factor of 4–20.

Many-body effects on Auger thermalization.—Figure 3 compares, for $\text{Cd}_{232}\text{Se}_{235}$, the results at room temperature of the single-particle (i.e., single Slater determinant, SP) approach (solid line), and the CI treatment (dashed line), for $\tau(h_s e_p \rightarrow h_n e_s)$, showing that many-body effects play a minor role in such decay. We find that the overall shape of the τ vs ΔE curves and the values of the lifetimes at resonance are very similar in the two approaches and that the results obtained at room temperature with multiple initial states (i.e., all three electron p states and both hole s states) do not differ significantly from the results at $T = 0$ around the calculated ΔE .

Auger thermalization in the presence of a spectator exciton.—Thermalization from e_p to e_s can also occur when other particles exist as *spectators* [Fig. 1(b)]. We find (Fig. 3) that the electron cooling lifetime calculated with CI at room temperature (dashed line) increases about 1 order of magnitude (for $T = 0$ the increase is of about 2 orders of magnitude) if a ground-state spectator exciton is present (long-dashed line) [22]. A possible explanation is that the correlation effects between the Auger carriers and the spectators lead to the formation of an Auger “dark” spin state with low Auger rate in the initial state Slater determinant subspace.

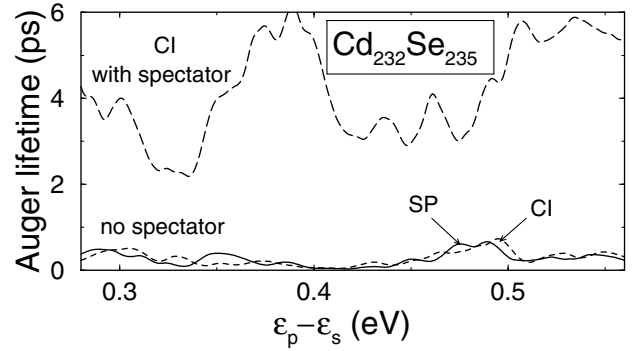


FIG. 3. *Electron cooling*: Auger lifetimes at $T = 300$ K calculated with EPM-1 within the single-particle (SP) approximation (solid line), and with CI, both in the absence (dashed line) and in the presence (long-dashed line) of a spectator ground state exciton. The initial states include all three electron p states and both hole s states, and the final states e_s and 30 hole states h_n with energy centered around $E_{n0} = \epsilon_{h_{s1}} - \epsilon_{e_p} + \epsilon_{e_s}$.

Auger biexciton recombination.—Figure 1(c): If we denote with τ_e the Auger lifetime for the process of exciton + electron \rightarrow electron [Fig. 1(e)], and with τ_h the process of exciton + hole \rightarrow hole [Fig. 1(f)], then we have

$$\frac{1}{\tau_{e-h}^{2 \rightarrow 1}} = \frac{2}{\tau_e} + \frac{2}{\tau_h}, \quad (5)$$

where the factor of 2 comes from the increased channel availability in the 2 exciton \rightarrow 1 exciton case. To calculate τ_e and τ_h , we use a single Slater determinant to represent $|i\rangle$ and $|f_n\rangle$ in Eq. (1), and we obtain

$$\frac{1}{\tau_e} = \frac{1}{\hbar} \sum_n \frac{\Gamma}{(\epsilon_{\text{gap}} - \epsilon_{e_n} + \epsilon_{e_s})^2 + (\Gamma/2)^2} \times |J(e_{s,\uparrow}, e_{s,\downarrow}; e_n, h_s) - J(e_{s,\downarrow}, e_{s,\uparrow}; e_n, h_s)|^2 \quad (6)$$

and

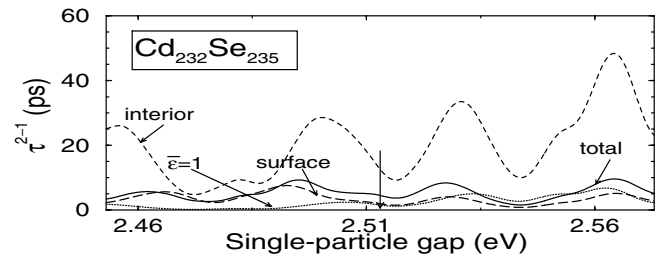


FIG. 4. Auger biexciton recombination lifetime $\tau_{e-h}^{2 \rightarrow 1}$ calculated with $\bar{\epsilon}(\mathbf{r}, \mathbf{r}')$ as in Eq. (3) (solid line), decomposed into its surface (long-dashed line) and bulk (dashed line) contributions, compared to $\tau_{e-h}^{2 \rightarrow 1}$ calculated with $\bar{\epsilon}(\mathbf{r}, \mathbf{r}') = 1$ (dotted line). All curves were calculated at $T = 0$ with EPM-1.

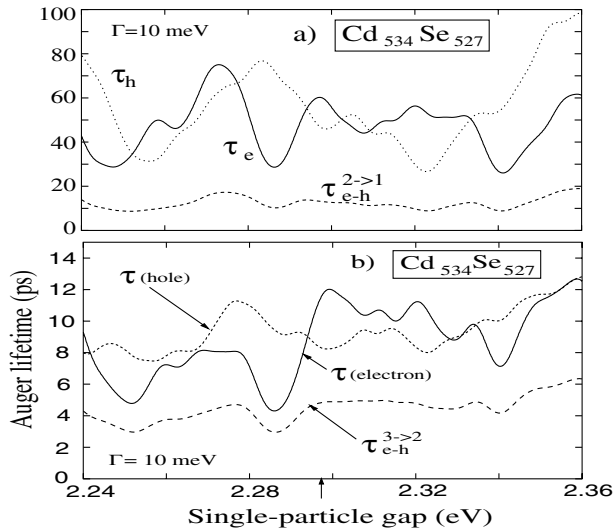


FIG. 5. Auger multiexciton recombination lifetimes: (a) $\tau_{e-h}^{2 \rightarrow 1}$ decomposed into the τ_e and τ_h contributions [see Eq. (5)]; (b) $\tau_{e-h}^{3 \rightarrow 2}$ together with its two contributions coming from a single hole and a single electron scattering. All lifetimes were calculated at $T = 0$ with EPM-2 and $\bar{\epsilon}(\mathbf{r}, \mathbf{r}') = 1$.

$$\frac{1}{\tau_h} = \frac{1}{\hbar} \sum_n \frac{\Gamma}{(\epsilon_{\text{gap}} + \epsilon_{h_n} - \epsilon_{h_s})^2 + (\Gamma/2)^2} \times |J(h_{s,\uparrow}, h_{s,\downarrow}; h_n, e_s) - J(h_{s,\downarrow}, h_{s,\uparrow}; h_n, e_s)|^2, \quad (7)$$

where the subscripts \uparrow, \downarrow indicate the spin-degenerate Kramer's doublets, and ϵ_{gap} is the single-particle energy gap [see Fig. 1(a)]. To calculate τ_e (τ_h) we have computed 60 electron (hole) states around the ideal energy $\epsilon_{\text{gap}} + \epsilon_{e_s}$ ($\epsilon_{\text{gap}} - \epsilon_{h_s}$). In order to determine the origin (surface or interior) of the Auger multiexciton recombination, we calculated $\tau_{e-h}^{2 \rightarrow 1}$ using the dielectric function of Eq. (3). The results for $\text{Cd}_{232}\text{Se}_{235}$ are presented in Fig. 4, where $\tau_{e-h}^{2 \rightarrow 1}$ is decomposed into surface [first and last terms on the right-hand side of Eq. (3)] and interior [second term on the right-hand side of Eq. (3)] contributions, and compared to $\tau_{e-h}^{2 \rightarrow 1}(\bar{\epsilon} = 1)$. Two features are important: (i) the closeness of the long-dashed and solid lines shows that the main contribution to $\tau_{e-h}^{2 \rightarrow 1}$ comes from the surface of the dot, and (ii) the ratio $f = \tau_{e-h}^{2 \rightarrow 1}(\bar{\epsilon}(\mathbf{r}, \mathbf{r}')) / \tau_{e-h}^{2 \rightarrow 1}(\bar{\epsilon} = 1)$ between the lifetime calculated with the screening of Eq. (3) and that obtained assuming $\bar{\epsilon}(\mathbf{r}, \mathbf{r}') = 1$ is ~ 2 . We find (i) and (ii) to hold for all dots and multiexciton recombination times considered. Figure 5(a) shows $\tau_{e-h}^{2 \rightarrow 1}$ for $\text{Cd}_{534}\text{Se}_{527}$, obtained assuming $\bar{\epsilon}(\mathbf{r}, \mathbf{r}') = 1$ and $\Gamma = 10$ meV, plotted together with its two components τ_e and τ_h , as a function of ϵ_{gap} , the actual value of which is indicated by a vertical arrow. Multiplying by f , according to Fig. 4, the biexciton decay lifetime [$\tau_{e-h}^{2 \rightarrow 1}(\bar{\epsilon} = 1) \sim 12$ ps] extracted from Fig. 5(a), yields $\tau_{e-h}^{2 \rightarrow 1} \sim 24$ ps for $\text{Cd}_{534}\text{Se}_{527}$. The calculated lifetimes of both dots (~ 24 ps for $\text{Cd}_{534}\text{Se}_{527}$ and ~ 5 ps for $\text{Cd}_{232}\text{Se}_{235}$) are

in excellent agreement with the experimental results of 22 and 6 ps [9] obtained for $R = 17$ and 12 \AA , respectively.

Triexciton Auger decay.—Figure 1(d): The values obtained for the lifetime as a function of the single-particle gap ϵ_{gap} , assuming $\bar{\epsilon}(\mathbf{r}, \mathbf{r}') = 1$, are shown in Fig. 5(b) for $\text{Cd}_{534}\text{Se}_{527}$. We see that $\tau_{e-h}^{3 \rightarrow 2}(\bar{\epsilon} = 1)$ is roughly 5 ps. This gives a ratio of $\tau_{e-h}^{2 \rightarrow 1} / \tau_{e-h}^{3 \rightarrow 2} = 2.4$, which is very close to the experimental value of 2.1 [9].

Our empirical pseudopotential calculations support the interpretation, in terms of Auger transitions, of many carrier dynamics experiments in CdSe quantum dots. Our methodology presents itself as a reliable tool to calculate the details of Auger processes in nanostructures.

The work at LBNL was supported by U.S. DOE, OER-BES, under Grant No. KC0203010, and at NREL by the U.S. DOE, OER-BES, Division of Materials Science.

- [1] V.I. Klimov, J. Phys. Chem. B **104**, 6112 (2000).
- [2] H. Benisty, C.M. Sotomayor-Torres, and C. Weisbuch, Phys. Rev. B **44**, 10945 (1991).
- [3] T. Inoshita and H. Sakaki, Phys. Rev. B **46**, 7260 (1992).
- [4] X.-Q. Li, H. Nakayama, and Y. Arakawa, Phys. Rev. B **59**, 5069 (1999).
- [5] S. Sauvage *et al.*, Phys. Rev. Lett. **88**, 177402 (2002).
- [6] V.I. Klimov and D.W. McBranch, Phys. Rev. Lett. **80**, 4028 (1998).
- [7] P. Guyot-Sionnest, M. Shim, C. Matranga, and M. Hines, Phys. Rev. B **60**, R2181 (1999).
- [8] A.I. Efros, V.A. Kharchenko, and M. Rosen, Solid State Commun. **93**, 281 (1995).
- [9] V.I. Klimov *et al.*, Science **287**, 1011 (2000).
- [10] J.H. Werner, S. Kolodinski, and H.J. Queisser, Phys. Rev. Lett. **72**, 3851 (1994).
- [11] A. Zunger, Phys. Status Solidi B **224**, 727 (2001).
- [12] J.L. Pan, Phys. Rev. B **49**, 11 272 (1994); **46**, 3977 (1992).
- [13] L.-W. Wang and A. Zunger, Phys. Rev. B **51**, 17 398 (1995).
- [14] L.-W. Wang and A. Zunger, Phys. Rev. B **53**, 9579 (1996).
- [15] A. Franceschetti, H. Fu, L.-W. Wang, and A. Zunger, Phys. Rev. B **60**, 1819 (1999).
- [16] L.-W. Wang, Phys. Rev. B **64**, R201107 (2001).
- [17] M. Takeshima, J. Appl. Phys. **43**, 4114 (1972); A. Haug and W. Ekardt, Solid State Commun. **17**, 267 (1975).
- [18] We tested the choice of the Auger basis by calculating $\tau(h_s e_{p1} \rightarrow h_n e_s)$ with 12 hole states with energy around $\epsilon_{h_s} - \Delta E$ and with the first 30 hole states, finding differences of less than 2%, within the single-particle approach.
- [19] Experimental energy loss rates for highly excited carriers yield an estimate for Γ around 10 meV [20].
- [20] D.J. Norris *et al.*, Z. Phys. D **26**, 355 (1993).
- [21] I. Mihalcescu *et al.*, Phys. Rev. B **51**, 17605 (1995); C. Delerue *et al.*, Phys. Rev. Lett. **75**, 2228 (1995).
- [22] In the single-particle treatment there is no difference between the Auger electron cooling lifetimes calculated with and without spectator exciton.